

Overirradiance conditions and their impact on the spectral distribution at low- and mid-latitude sites

Marco Antonio Zamalloa-Jara ^{a,b,*}, Miguel Ángel Sevillano-Bendezú ^a, Carolin Ulbrich ^c, Gustavo Nofuentes ^d, Rolf Grieseler ^a, Jan Amaru Töfflinger ^{a,*}

^a Materials Science and Renewable Energies Group, Science Department, Pontificia Universidad Católica del Perú, Av. Universitaria 1801, San Miguel, 15088 Lima, Peru

^b Departamento Académico de Física, Facultad de Ciencias, Universidad Nacional de San Antonio Abad del Cusco, Av. De La Cultura 733, Cusco, Peru

^c Helmholtz-Zentrum Berlin für Materialien und Energie GmbH, 12489 Berlin, Germany

^d IDEA Research Group, University of Jaén, Campus de Las Lagunillas, 23071 Jaén, Spain



ARTICLE INFO

Keywords:

Solar resource
Overirradiance
Cloud enhancement
Solar spectrum
Average photon energy

ABSTRACT

Lately, the photovoltaics community has shown an increased interest in overirradiance conditions as there is the possibility that such conditions might lead to malfunctions in photovoltaic systems. Varying irradiance levels, recurrence, and duration of such conditions have been reported worldwide, but experimental studies on the spectral distribution of overirradiance conditions are still scarce. This work analyses measured spectral irradiance of overirradiance conditions along with spectra under clear and cloudy sky conditions in three different sites at low- (Lima-Peru) and mid-latitudes (Madrid-Spain and Berlin-Germany) collected for two years. The Average Photon Energy (APE) was used as a representative index of the spectral distribution. For each site, taking the APE under clear sky into account as a reference, it could be shown that the spectra under cloudy skies are blue-shifted, and the overirradiance spectra are red-shifted independently of the location. The red-shift is proportional to the irradiance enhancement intensity. In addition, all sites have different degrees of blue-shift for cloudy skies, with Lima, Madrid, and Berlin exhibiting a difference in APE compared to clear sky conditions of 17 meV, 38 meV, and 43 meV on average, respectively. This difference in APE for the overirradiance conditions compared to clear sky conditions is also independent of the location with a mean value of (8 ± 1) meV. These spectral shift observations experimentally confirm prior assumptions that overirradiance conditions predominantly cause an enhancement of the direct spectral irradiance.

1. Introduction

In-depth knowledge of Overirradiance (OI) conditions' origin has gained an increased interest in the Photovoltaic (PV) community due to their potential technical and economic effects on the installation of PV and concentrator PV power plants [1–6]. Recent studies have shown that OI conditions lasting more than one minute and at ambient temperatures above 30 °C can affect the operation of protection systems, heat and damage fuses, and cause inverter overloads [1,2,6,7]. On the one hand, strings exposed to long OI conditions may operate with high currents, which associated with high fuse operating temperatures, might cause string fuses to blow [2]. On the other hand, the increase of the electrical current in photovoltaic generators causes the output power to exceed the inverters nominal power, leading to inverter overload losses, particularly for undersized inverters [2,6]. Taking into consideration the

impact of OI conditions on the operation and safety of PV systems may require rethinking the optimal design of PV systems in terms of inverter sizing factor and fuse rating [8].

Commonly, OI conditions correspond to situations in which the ground-based Global Horizontal Irradiance (GHI) exceeds the GHI expected for a cloud-free sky or Clear Sky (CS) [1,6,9–16]. In some cases, events with GHI higher than the solar constant ($\sim 1361.1 \text{ W/m}^2$) [17] could be observed, which are called extreme OI events [2,9,18–22]. OI and extreme OI events have usually been observed in the presence of thin or thick fragmented clouds around the solar disk, as evidenced by sky images reported in previous investigations worldwide [1,2,5,14,21,23]. In 1968 Norris [24] proposed that the classification of clouds by transmissivity could be invalid due to the reflection of solar irradiance from the edges and sides of the fragmented clouds, which was evident when the irradiance that reached the Earth's surface was higher

* Corresponding authors.

E-mail addresses: marco.zamalloa@unsaac.edu.pe (M.A. Zamalloa-Jara), japalominot@pucp.edu.pe (J.A. Töfflinger).

than the one under CS conditions. Additionally, OI conditions have been associated with reflections at the edges of the fragmented clouds around the solar disk. Subsequently, Wen et al. in 2001 [25] showed that the OI depends furthermore on the mean cloud-free distance. An OI origin hypothesis proposed that they are produced by reflection on the edges of the broken clouds that reveal the solar disk or partially cover it, as Ruther et al. showed [5]. Yordanov et al. presented an alternative hypothesis using sky images where thin clouds that cover the solar disk produce OI conditions due to a strong forward Mie scattering inside the clouds [16].

Due to the scarcity of sky images, alternative identification methods are applied that imply using the clearness index or the clear sky index to identify overirradiance conditions. Additionally, they allowed differentiating between clear sky, cloudy sky (Clo), and partly cloudy sky [26–28]. Consequently, there is no unique consensus in identifying an OI condition. Thus, the occurrence of OI conditions and their effects on PV systems have not yet been well quantified, mainly because of this lack of precise and quantitative information on OI conditions. Indeed, researchers have suggested that the irradiance sampling (or averaging) frequencies of OI conditions should be one per second or higher to measure the peak irradiance, their frequency and duration [1,7,23].

Simulation models such as the Monte Carlo radiative transfer model have been developed to understand the mechanism and cause of OI [29,30] and correlate them to the measured data. However, radiative transfer and other models still need to be enhanced as they differ significantly from the experimental observations. For example, many of them do not yet consider the non-linear effects of the cloud optical depth and zenith angle [29]. On the other hand, a more in-depth consideration of Mie scattering might be required [30]. So far, models have been limited to analyzing a single wavelength [29–32].

Experimental and modeling studies could benefit from observing a broader spectral distribution of OI conditions to contribute to understanding and defining their origin. Few works have been dedicated to analyzing the UV spectral region of OI conditions, demonstrating an enhancement in that region [31,33,34]. In [22], we previously reported on the impact of extreme overirradiance events on the spectral distribution; however, limited to Lima, Peru, and a few examples. After an extensive review of the literature, no other works were found that have analyzed broader spectral regions for OI conditions.

The present work compares the spectral distribution of OI conditions in Lima, Madrid, and Berlin with the spectral distribution under CS and Clo conditions during the principal sunlight hours at each location. This work aims to provide information on the OI spectral distribution behavior at low- and mid-latitudes to shed more light on the understanding of OI conditions.

2. Materials and methods

2.1. Experimental spectral data

The present work analyzed the measured spectral data from three different sites. Table 1 summarizes the characteristics, including the latitude and longitude of each site and the used spectroradiometer, tilt and azimuth angles, and sampling interval. The first site, Lima, Peru, is

Table 1
Geographical location, tilt and azimuth angles of the spectroradiometers.

Site	Latitude (°)	Longitude (°)	Spectroradiometer	Tilt and azimuth angles (°)	Sampling interval (s)
Lima	-12.07	-77.08	EKO-MS711	20 and 0	40
Madrid	40.33	-3.77	EKO-MS700	30 and 180	300
Berlin	52.43	13.52	EKO-MS711	35 and 180	300

located at a low latitude in the terrestrial southern hemisphere. The data were obtained at the Photovoltaic Research Laboratory of the Pontificia Universidad Católica del Perú. The other two laboratories are located at mid-latitudes in the northern hemisphere. One measuring station is located in Madrid, Spain, and the spectral data was provided by the IDEA Research Group at the University of Jaén in Spain. The other station was located in Berlin, Germany, and belongs to the Helmholtz Zentrum Berlin für Materialien und Energie.

In Lima and Berlin, the spectra were measured with an EKO MS711 spectroradiometer (optical resolution FWHM < 7 nm, and wavelength accuracy ±0.2 nm), and in Madrid, with an EKO MS700 (optical resolution FWHM < 10 nm, and wavelength accuracy ±0.3 nm). All spectroradiometers were calibrated and measured the spectral distribution of solar irradiance in W/m²/nm, ranging from 350 to 1050 nm. They are installed on tilted surfaces with a tilt angle of 20°, 30°, and 35° for Lima, Madrid, and Berlin, respectively. In Lima, the spectral data were recorded every 40 s, while in Madrid and Berlin, every 5 min.

To obtain a sufficient amount of data for statistical analysis, despite the relatively long sampling intervals of 40 s and 300 s, two years of measured spectral data were scanned for OI conditions for each site. In Lima, the observation period was from May 2019 to April 2021, and 17 days with CS, Clo, and OI conditions were found. Whereas for Madrid, the measuring period was from January 2016 to December 2017, with 10 days found, and for Berlin, from January 2019 to December 2020, with 17 days found.

2.2. Spectral data extrapolation for irradiance

The spectra in Lima were measured synchronously with horizontal and tilted irradiance using pyranometers. However, Madrid and Berlin's spectral and irradiance data were not synchronized. Therefore, to estimate the irradiance corresponding to a spectrum measured with the spectroradiometers, we applied Neves et al. [35] and Martin and Ruiz's [36] extrapolation methods to expand the spectral range from 280 nm to 4000 nm and then integrated them. The Neves et al. method is performed in the ultraviolet (UV) region from 280 nm to 350 nm [35], and the Martin and Ruiz's extrapolation method is applied in the infra-red (IR) region from 1050 nm to 4000 nm [36]. Thus, the experimental global tilted irradiance (GTI) in W·m⁻² is calculated according to Eq. (1):

$$GTI = \frac{\int_{280}^{350} E^*(\lambda) d\lambda}{\int_{350}^{400} E^*(\lambda) d\lambda} \int_{350}^{400} E(\lambda) d\lambda + \int_{350}^{1050} E(\lambda) d\lambda + \frac{\int_{1050}^{4000} E^*(\lambda) d\lambda}{\int_{700}^{1050} E^*(\lambda) d\lambda} \int_{700}^{1050} E(\lambda) d\lambda \quad (1)$$

where $E(\lambda)$ is the measured solar spectral irradiance and $E^*(\lambda)$ is the solar spectral irradiance of the AM1.5G reference spectrum in W·m⁻²·nm⁻¹. In [22], we demonstrated that the experimental GTI estimated from the integrated, extrapolated spectrum is a very good approximation of the GTI measured with a synchronized, tilted pyranometer. Hence, we also applied the method mentioned above for Lima to estimate the experimental GTI from the spectra for consistency.

2.3. Identification of CS, OI, and Clo conditions

To differentiate the OI from the CS and Clo conditions, we first simulated the global tilted irradiance under CS conditions for all days under study. For this, we used the PVLIB Python library [37–39], where the simulated global tilted CS irradiance is defined as plane of array irradiance (POA). For consistency, this work assumes the same definition. The PVLIB Python library calculated the POA irradiance from the simulated GHI using a transposition model [38–41]. However, the POA irradiance given by PVLIB Python library may not correspond directly to an experimental GTI for CS, as pointed out in [10], due to the uncertainties in the transposition models to estimate GTI. Indeed, during this experimental campaign, we observed that the POA irradiance predominantly differed from the experimental GTI for CS days. Therefore, a

methodology is proposed for adjusting the POA irradiance to the experimental GTI for CS data. We define the corrected POA irradiance as the simulated CS Global Tilted Irradiance (GTI^{*}).

The procedure consists of making a linear fit between the experimental GTI data for CS conditions and their corresponding POA irradiance values. Using the slope and intercept obtained by the linear fit, the simulated GTI^{*} is defined as expressed by Eq. (2):

$$GTI^* = \frac{POA - b}{m} \quad (2)$$

where b is the intercept and m is the slope of the linear fit. The tilted-clear-sky index k^* is then defined as shown in Eq. (3):

$$k^* = \frac{GTI}{GTI^*} \quad (3)$$

According to earlier publications, an irradiance value with $k^* > 1.05$ can be defined as corresponding to an OI condition. Additionally, this index has the advantage of allowing the definition of Clo conditions for irradiance values with $k^* < 0.95$; otherwise, irradiance values for $0.95 \leq k^* \leq 1.05$ are considered to have CS conditions [28,42].

2.4. Analysis of solar spectra

The Average Photon Energy (APE) is the most widely used index to characterize spectral irradiance distribution [27,43–45]. It was proposed by Jardine et al. in 2002 [46] and served to describe quantitatively if a spectrum is red-rich or blue-rich concerning another spectrum used as a reference [27,47]. The APE in electron volts (eV) is calculated using the following equation in the spectral range from 350 nm to 1050 nm:

$$APE = \frac{\int_{350}^{1050} E(\lambda) d\lambda}{q \int_{350}^{1050} \Phi(\lambda) d\lambda} \quad (4)$$

where $E(\lambda)$ is the measured solar spectral irradiance, $\Phi(\lambda)$ is the photon flux density, and q is the electron charge [27,47,48]. The APE for the AM1.5G spectrum is 1.876 eV, considering this wavelength range. This study uses the APE to characterize the spectral distribution related to CS, Clo, and OI conditions. The APE of the OI and Clo conditions indicated if the spectra are red-rich-shifted or blue-rich-shifted with respect to the APE at CS.

The spectral distribution and respective APE are sensitive to the air mass (AM) variation. When the AM increases, the spectral distribution becomes red-rich, as reflected by an APE decrease. Low elevation angles lead to higher AM, especially in the early morning and in the later afternoon, which differ significantly from the AM at the highest elevation at noon. Therefore, to reduce the impact of the AM variation on the APE variation throughout each day in a year, the data corresponding to angles of incidence (AOI) [49,50] higher than 30° is filtered out in this work so that the mean variation of the APE is a few millielectron volts

(meV) and less than the variation produced by the OI conditions. Furthermore, as spectroradiometers are on tilted planes, the influence of the specular albedo on the spectral distribution may be reduced [9,51] at lower AOI.

3. Results and discussion

3.1. Clear sky days

In Fig. 1, the graphs of the irradiances as a function of time are shown for days with CS conditions comparing Lima, Madrid, and Berlin. The plotted irradiances correspond to the experimental GTI and simulated GTI^{*}, as well as the POA irradiance obtained directly using PVLIB-Python. As can be seen, with the proposed adjustments, the simulated GTI^{*} and experimental GTI are in good agreement.

To estimate the impact of the AOI and, thus, AM on the APE, we depict in Fig. 2 the APE, the tilted-clear-sky index k^* , and the experimental GTI as functions of the AOI for the same CS days presented in Fig. 1.

In the three sites, the CS days show that both APE and GTI decrease as the AOI increases. This is because higher AOI correspond to higher air mass AM and, consequently, a higher absorption and scattering of photons, resulting in lower irradiance and fewer high-energy photons. The tilted-clear-sky index k^* remains relatively close to unity and lies confined within 1.00 ± 0.05 , as expected for a CS day.

To better distinguish the impact of OI conditions on APE from the impact of the AOI, we first had to minimize the impact of AOI changes on APE changes. For this, we limited the AOI observation window to 30°. The APE variation for angles $< 30^\circ$ of the AOI are ~ 3 meV for Lima and Madrid and ~ 2 meV for Berlin, as indicated by the purple lines in Fig. 2.

3.2. Days with CS, Clo, and OI conditions

Fig. 3 shows the experimental GTI and simulated GTI^{*} irradiances for days with CS, Clo, and OI conditions. In all cases, the results are plotted for irradiances higher than 400 W/m^2 . Note that the experimental GTI and simulated GTI^{*} irradiances matched quite well for CS conditions.

The distinction between CS, Clo, and OI conditions is based on the tilted-clear-sky index k^* defined in Eq. (3). All GTI values that show $k^* \geq 5\%$ above the simulated GTI^{*} correspond to OI conditions, and those with 5% below the simulated GTI^{*} correspond to Clo conditions. In contrast, those between $\pm 5\%$ are considered CS conditions.

Fig. 4 shows the spectral irradiances corresponding to CS, Clo, and OI conditions exemplarily marked with circles in Fig. 3. In all three locations, the spectral irradiance of OI conditions is higher than in the CS conditions in the entire spectral range. Furthermore, a more significant increase in photon number in the visible (390 nm – 770 nm) and near-infrared (> 770 nm) regions could be observed, which explains why the APE value for OI conditions is lower than for the CS condition. On the contrary, the APE for the Clo conditions is higher than the APE for CS

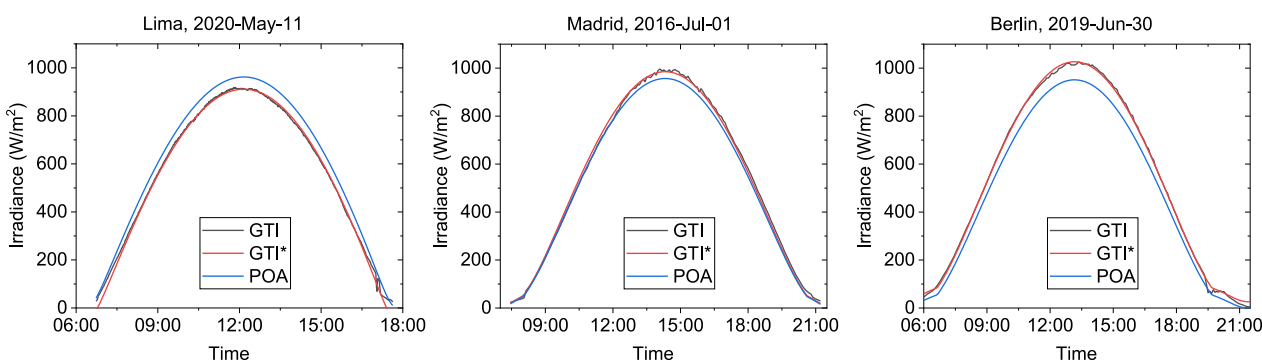


Fig. 1. Comparison of POA irradiance, experimental GTI, and simulated GTI^{*} for exemplary clear sky (CS) days in Lima, Madrid, and Berlin.

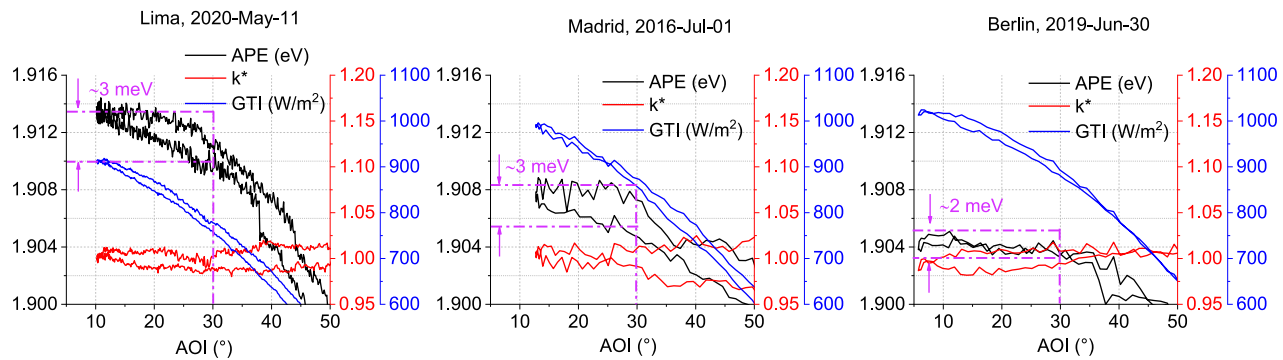


Fig. 2. APE, k^* , and GTI as functions of AOI for the days shown in Fig. 1 for Lima, Madrid, and Berlin.

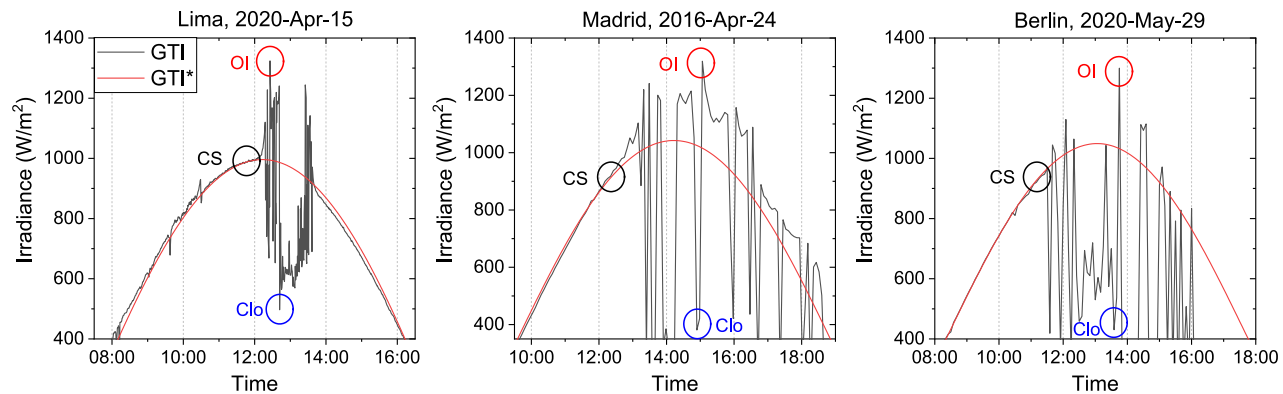


Fig. 3. Experimental GTI and simulated clear-sky GTI* to identify CS, Clo, and OI events, for exemplary days in Lima, Madrid, and Berlin. The circles mark exemplary CS, Clo and OI conditions to show their spectral irradiance in Fig. 4.

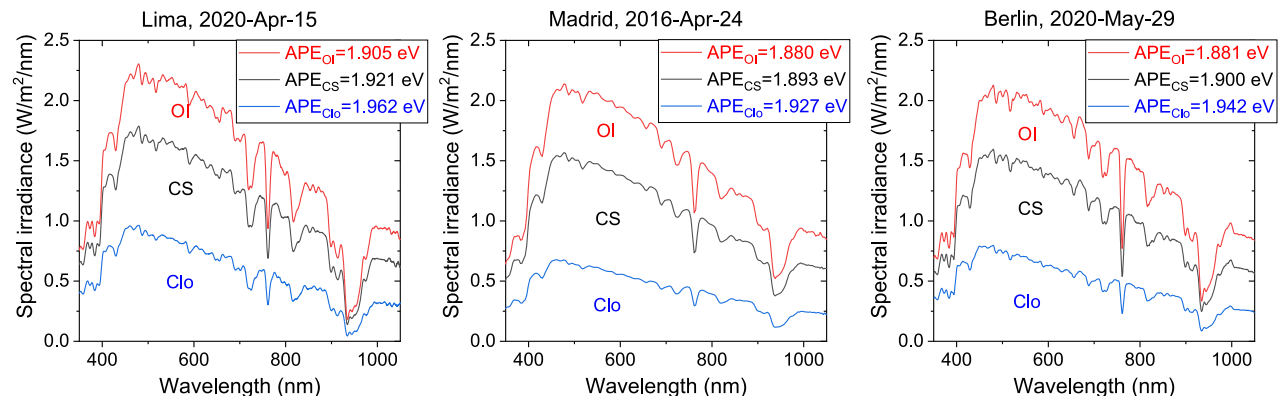


Fig. 4. Spectral irradiances corresponding to the CS, Clo, and OI conditions selected and shown in Fig. 3 for Lima, Madrid, and Berlin.

conditions.

3.3. Impact of OI conditions on the spectral distribution

In Fig. 5(a), the experimental GTI irradiances and APE, corresponding to the AOI range of 30°, are shown as a function of time throughout a day with CS, Clo, and OI conditions in Lima, Madrid, and Berlin. The APE variations for CS conditions remain below ~ 3 meV in the chosen AOI range. For OI conditions, the APE decreases, while for Clo conditions, the APE increases. It is essential to mention that lower APE values correspond to the most extreme OI events, which shows a clear red-shift with respect to CS APE. Likewise, the Clo condition present a blue shift since their corresponding APE is higher than for CS. This last observation corroborates the results obtained by Paudyal et al. and

Neves et al. [26,27].

Fig. 5(b) shows the APE as a function of the tilted-clear-sky index k^* for CS, Clo, and OI conditions during the respective day of observation for an AOI below 30°. The entire data set for each day and location plotted as APE vs. k^* can be found in the Supporting Information (SI). The range of APE values for Clo conditions (blue) is generally more extensive than the range of OI conditions (red) because the irradiance in Clo conditions can drop much lower than the OI conditions can rise compared to the CS, as shown for Madrid in Fig. 5 (b) and Fig. 5 (a). In short, overirradiance conditions show a red-shift proportional to k^* . Interestingly, there is a quasi-linear relationship between the APE values and k^* for Lima and Madrid, i.e., high APE for low k^* values, and the APE value decreases with increasing k^* . For Lima, this quasi-linear behavior is consistent for almost all analyzed days shown in the SI,

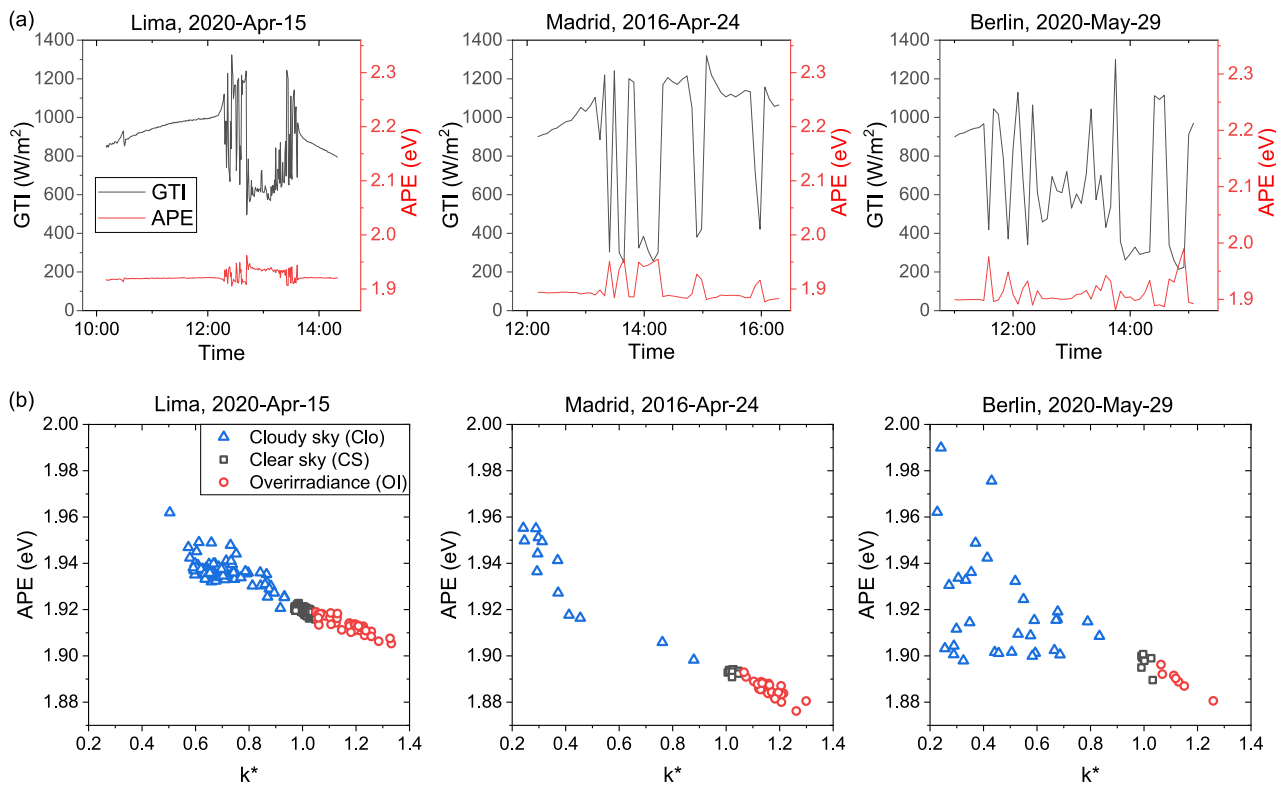


Fig. 5. (a) Experimental GTI and APE as a function of time, showing that APE and GTI are inversely proportional for all OI and Clo conditions. (b) APE as a function of k^* showing red-shifts for OI and blue-shifts for Clo. (For interpretation of the references to colour in this figure legend, the reader is referred to the web version of this article.)

with only a few days showing a slightly larger dispersion of APE for Clo conditions but rarely reaching k^* values below 0.4. Whereas for Madrid, most days in the SI show a more significant dispersion of the APE for Clo conditions, particularly at k^* values below 0.4. In Fig. 5(b), for Berlin, this APE – k^* quasi-linear relationship is only apparent for OI conditions, not Clo conditions where the APE values are more dispersed. In the SI, this behavior is observed for most days in Berlin. Understanding this discrepancy of the APE – k^* relationship for Clo conditions requires a closer analysis of the type of clouds, which is out of the scope of this work.

During the OI condition, the k^* value is an indicator of the intensity of the irradiance enhancement. This APE – k^* quasi-linear relationship indicates that the higher the enhancement, the more red-shifted the spectral distribution. An explanation for this red-shift could be that the OI condition predominantly enhances the direct irradiance component of the global irradiance [9]. In [52], the measured diffuse and direct components of the global solar spectrum were blue-rich and red-rich, respectively. Hence, enhancing predominantly the direct component causes a red-shift in the global spectral irradiance during an OI condition.

Next, we analyzed the reproducibility and statistics of the blue- and red-shift during Clo and OI conditions, respectively, in Lima, Madrid, and Berlin. In all cases, similar quasi-linear relationships between APE and k^* were observed as in Fig. 5(b). Fig. 6(a) shows the mean APE values with a 95% confidence interval of all the days that presented CS, Clo, and OI conditions during the noon hours at AOI < 30°. The number of days with OI conditions was considerably higher than presented here. However, to follow the procedure described above, we limited the analysis to days that demonstrated CS, Clo, and OI conditions within the AOI observation window, as CS data is required to obtain GTI* with the proposed methodology. Hence, days with OI conditions but without or too few CS conditions were discarded. Furthermore, it should be noted that as OI conditions often occur for a very short duration, it might be

possible that they could not be observed during the measurement, especially in Madrid and Berlin, where the measurement period was 5 min. However, the acquired days with CS, Clo, and OI data are sufficient for statistical analysis.

In Fig. 6(a), the mean APE values and their confidence intervals for CS, Clo, and OI conditions do not overlap, except for a few cases in Madrid, indicating that the respective blue- and red-shifted APEs are statistically different from CS APE. The mean APE values for CS vary according to the season and thus the day of the year, as shown by Jardine and Minemoto [46,53], but they remain below the mean value for Clo and above the mean value for OI.

Regarding the APE values for CS conditions in each city, as shown in Fig. 6(a), on average, the APE of Lima is higher than that of Madrid and Berlin, which can be attributed to Lima's closer proximity to the equator and, thus, lower air mass around noon hours. On the other hand, the dispersion and the mean value of the APE for Clo conditions are higher for Berlin and Madrid than for Lima, which may be due to atmospheric conditions specific to each place, such as the type of clouds, among others.

Fig. 6(b) shows the difference (Δ APE) between the OI and CS mean APE, and between Clo and CS mean APE. A positive Δ APE indicates a red-shift, and a negative Δ APE a blue-shift of the solar spectrum. Cloudy conditions in Madrid tend to blue-shift the spectrum further than in Lima, whereas for Berlin the blue-shift is more dispersed, with some days showing the strongest blue-shift among the three sites. For Lima Δ APE for CS-Clo shows only a small variability of the type of clouds for all observed days.

Fig. 7 summarizes the statistics of the spectral analysis throughout the experimental campaign. In Fig. 7(a), the box plots represent the statistical distribution of the APE values presented in Fig. 6(a) in each site for the days with CS, OI, and Clo conditions and AOI < 30°. Lima's mean CS APE value is higher than Madrid's and Berlin's due to its proximity to the equator. The blue-shifted mean Clo APE values do not

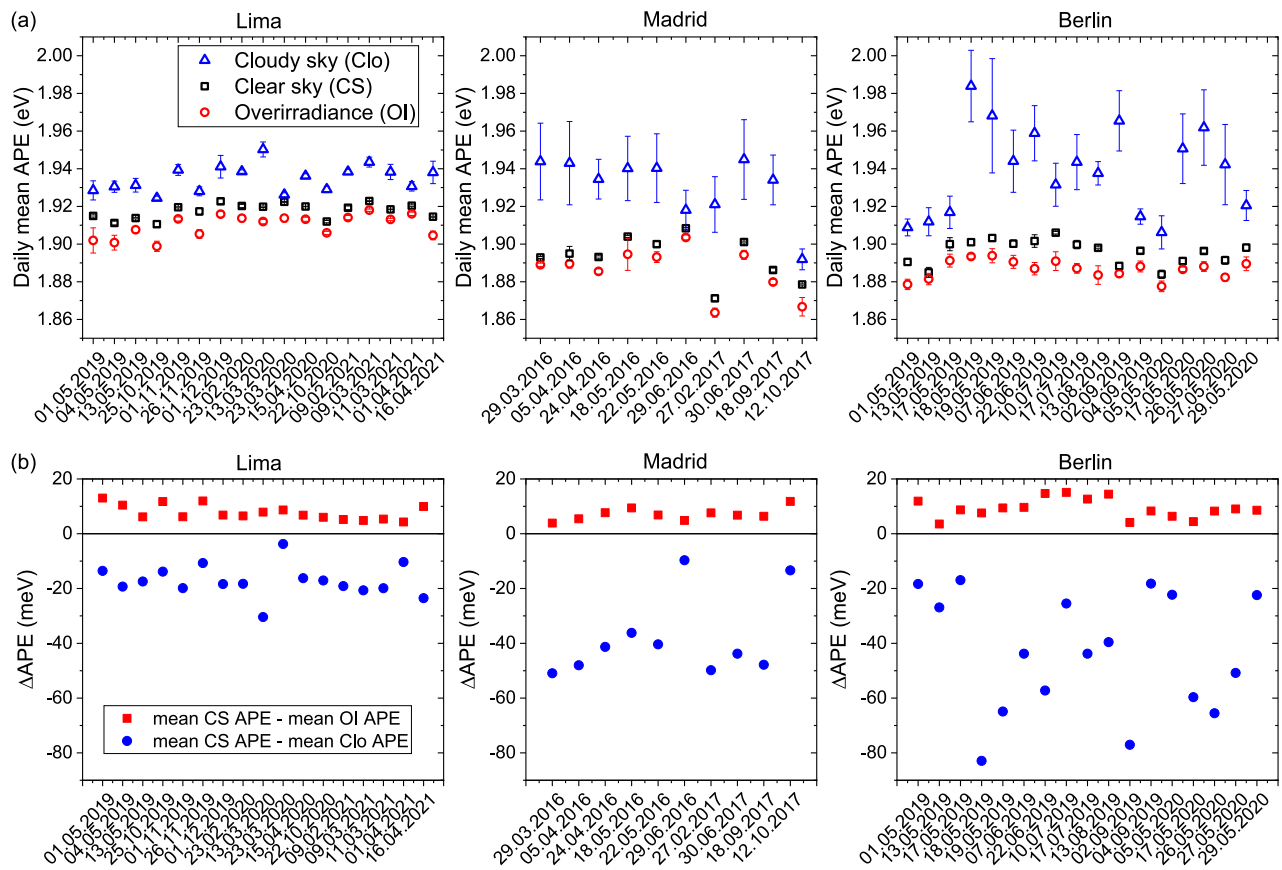


Fig. 6. (a) Daily mean APE values for CS, OI and Clo conditions with error bars corresponding to 95% confidence intervals. (b) Daily difference between mean APE values for OI and Clo concerning CS.

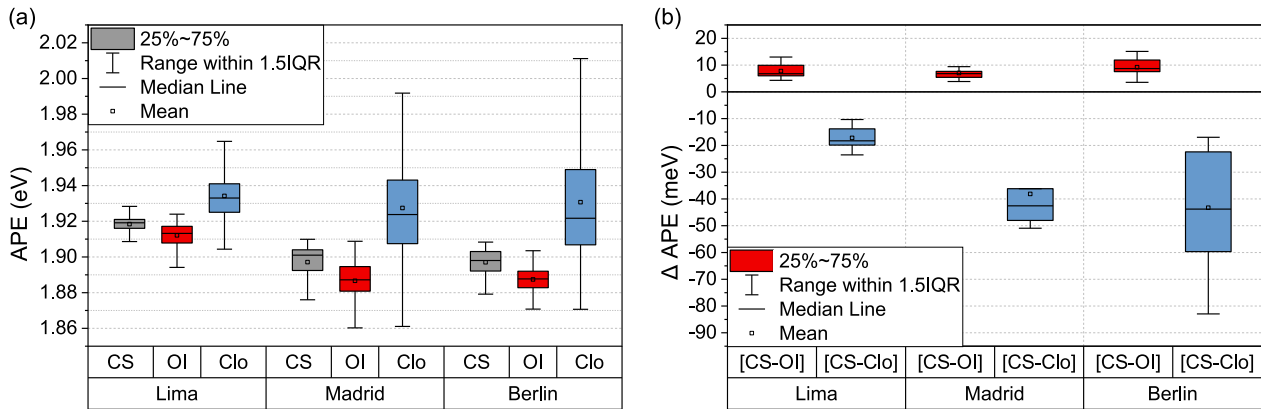


Fig. 7. (a) Boxplots of APE values for CS, OI and Clo conditions. (b) Boxplots of daily differences between mean APE values for OI and Clo concerning CS.

differ considerably between sites, hence, may be independent of the CS APE. However, their dispersion varies considerably from site to site. This different dispersion of the Clo APE data might represent the variety of cloud types, cloudiness, and other atmospheric factors in the respective sites. On the other hand, the red-shifted mean OI APE values seem to depend on the site's mean CS APE.

Table 2
Mean of ΔAPE for OI and Clo conditions concerning CS.

	Lima	Madrid	Berlin
Mean[ΔAPE(CS-Clo)] (meV)	-17	-38	-43
Mean[ΔAPE(CS-OI)] (meV)	8	7	9

Fig. 7(b) shows the boxplots of the daily ΔAPE in **Fig. 6(b)**, and **Table 2** summarizes the mean ΔAPE. The mean ΔAPE for Clo conditions in Lima is the smallest, indicating the least blue-shift, and negligible dispersion. Madrid and Berlin show similar mean ΔAPE for Clo conditions. The mean ΔAPE for Clo conditions in Berlin is more than double that of Lima, indicating that cloudy conditions in Berlin cause a considerable further blue-shift of the CS global irradiance. Interestingly, the mean ΔAPE for OI conditions is very similar in the three sites, with 8, 7, and 9 meV for Lima, Madrid, and Berlin, respectively, suggesting that the cause of these OI events are of similar nature and, thus, site-independent.

4. Conclusions

This work investigated the impact of clouds on the clear-sky solar spectral irradiance near noon hours at three different sites, a low-latitude location in Lima, Peru, and two mid-latitude locations in Madrid, Spain, and Berlin, Germany. From two years of spectral data, clear sky, cloudy sky, and overirradiance conditions were categorized by the tilted-clear-sky index, and the average photon energy quantified their spectral distribution.

Two key findings were presented: First, a general quasi-linear trend between the average photon energy and the tilted-clear-sky index, with cloudy sky conditions causing a blue-shift and overirradiance conditions causing a red-shift of the clear sky spectral distribution. In particular, for overirradiance conditions, the quasi-linear relationship indicates that the caused red-shift increases with the intensity of the cloud enhancement.

Second, the blue-shifted spectra of cloudy-sky conditions result in similar spectral distributions independent of the location, as shown by their similar mean average photon energies for each site. The red-shift caused by overirradiance conditions results in different spectral distributions, depending on the average photon energy of the clear sky. However, the energy red-shift of (8 ± 1) meV is very similar in the three locations, indicating that similar, site-independent processes may cause the overirradiance.

This red-shift of the global spectral irradiance caused by the overirradiance conditions can be explained by a predominant enhancement of the direct irradiance component [8], assuming a red-rich direct spectral distribution [50]. We encourage the very few laboratories that simultaneously measure global, direct, and diffuse spectral irradiance to perform a similar analysis of the overirradiance spectra to confirm this hypothesis.

Finally, these spectral shift observations may help improve current models to better understand the physical processes during such cloud-enhancing events.

Declaration of Competing Interest

The authors declare that they have no known competing financial interests or personal relationships that could have appeared to influence the work reported in this paper.

Acknowledgments

The authors thank the financial support granted by CONCYTEC through PROCIENCIA contract N°236-2015-FONDECYT, CONCYTEC through PROCIENCIA and The World Bank contract N°013-2020-FONDECYT-BM, the University of Jaen through “Ayudas de la EDUJA para la realización de tesis doctorales en régimen de cotutela internacional”, the Spanish Science and Innovation Ministry and the ERDF within the frame of the project ‘Estimación de la energía generada por módulos fotovoltaicos de capa delgada: influencia del espectro’ under expedient code ENE2008-05098/ALT, the “Red Peruana de Universidades”, the Academic Office of Institutional Affairs and Vicechancellorship for Research (PI0936) of the Pontificia Universidad Católica del Perú, and the Vicechancellorship for Research of the Universidad Nacional de San Antonio Abad del Cusco through the program “Yachayninchis wiñarinanpaq”.

Appendix A. Supplementary data

Supplementary data to this article can be found online at <https://doi.org/10.1016/j.solener.2023.05.010>.

References

- [1] Braga M, de Oliveira AKV, Burnham L, et al. Solar Over-Irradiance Events: Preliminary Results from a Global Study. In: 2020 47th IEEE Photovoltaic Specialists Conference (PVSC). 2020, pp. 2764–2770.
- [2] do Nascimento, L.R., de Souza Viana, T., Campos, R.A., Rüther, R., 2019. Extreme solar overirradiance events: Occurrence and impacts on utility-scale photovoltaic power plants in Brazil. *Sol. Energy* 186, 370–381.
- [3] Järvelä, M., Lappalainen, K., Valkealahti, S., 2020. Characteristics of the cloud enhancement phenomenon and PV power plants. *Sol. Energy* 196, 137–145.
- [4] Ruiz-Arias, J., Guemard, C., 2015. Solar resource for high-concentrator photovoltaic applications. In: Green Energy and Technology, pp. 261–302.
- [5] Rüther, R., Nascimento, L.R.d., Campos, R.A., Goodfield, D., 2017. Performance assessment issues in utility-scale photovoltaics in warm and sunny climates. *Renew. Energy Environ. Sustain.* 2, 35.
- [6] Toreti Scarabelot, L., Arns Rampinelli, G., Rambo, C.R., 2021. Overirradiance effect on the electrical performance of photovoltaic systems of different inverter sizing factors. *Sol. Energy* 225, 561–568.
- [7] Martins, G.L., Mantelli, S.L., Rüther, R., 2022. Evaluating the performance of radiometers for solar overirradiance events. *Sol. Energy* 231, 47–56.
- [8] Wang, B., Jiang, S., Tan, Z., 2023. Analysis of photovoltaic system under overirradiation conditions in arid climate. *Int. J. Green Energy* 20 (5), 465–476.
- [9] Guemard, C.A., 2017. Cloud and albedo enhancement impacts on solar irradiance using high-frequency measurements from thermopile and photodiode radiometers. Part 1: Impacts on global horizontal irradiance. *Sol. Energy* 153, 755–765.
- [10] Guemard, C.A., 2017. Cloud and albedo enhancement impacts on solar irradiance using high-frequency measurements from thermopile and photodiode radiometers. Part 2: Performance of separation and transposition models for global tilted irradiance. *Sol. Energy* 153, 766–779.
- [11] Iman, R.H., Chu, Y., Coimbra, C.F.M., 2016. Cloud enhancement of global horizontal irradiance in California and Hawaii. *Sol. Energy* 130, 128–138.
- [12] Y.K. Ramgolam, K.M.S. Soyjaudah, Enhanced Insolation and Global Irradiance in Near-tropic Region. In: *Proceedings of the EuroSun 2014 Conference*. Aix-les-Bains, France: International Solar Energy Society, pp. 1–7.
- [13] Tapakis, R., Charalambides, A.G., 2014. Enhanced values of global irradiance due to the presence of clouds in Eastern Mediterranean. *Renew. Energy* 62, 459–467.
- [14] C. Tiba, S. Silva Leal da. Enhancement of UV radiation by cloud effect in NE of Brazil. *Int. J. Photoenergy* 2017; 2017: e8107435.
- [15] Venkatakrishnamoorthy, T., Reddy, G.U., 2019. Cloud enhancement of NOAA multispectral images by using independent component analysis and principal component analysis for sustainable systems. *Comput. Electr. Eng.* 74, 35–46.
- [16] G.H. Yordanov, O.-M. Midtgård, T.O. Saetre, et al. Overirradiance (cloud enhancement) events at high latitudes. In: *2012 IEEE 38th Photovoltaic Specialists Conference (PVSC) PART 2*. 2012, pp. 1–7.
- [17] Guemard, C.A., 2018. A reevaluation of the solar constant based on a 42-year total solar irradiance time series and a reconciliation of spaceborne observations. *Sol. Energy* 168, 2–9.
- [18] Almeida, M.P., Zilles, R., Lorenzo, E., 2014. Extreme overirradiance events in São Paulo, Brazil. *Solar Energy* 110, 168–173.
- [19] de Andrade, R.C., Tiba, C., 2016. Extreme global solar irradiance due to cloud enhancement in northeastern Brazil. *Renew. Energy* 86, 1433–1441.
- [20] Piacentini, R.D., Salum, G.M., Fraidenraich, N., Tiba, C., 2011. Extreme total solar irradiance due to cloud enhancement at sea level of the NE Atlantic coast of Brazil. *Renew. Energy* 36 (1), 409–412.
- [21] Yordanov, G.H., Saetre, T.O., Midtgård, O.-M., 2015. Extreme overirradiance events in Norway: 1.6 sun measured close to 60°N. *Sol. Energy* 115, 68–73.
- [22] M.A. Zamalloa Jara, H. Berg, L.A. Conde, et al. Extreme overirradiance events and their spectral distribution in Lima, Peru. *J. Phys.: Conf. Ser.* 2021; 1841: 012006.
- [23] Castillejo-Cuberos, A., Escobar, R., 2020. Detection and characterization of cloud enhancement events for solar irradiance using a model-independent, statistically-driven approach. *Sol. Energy* 209, 547–567.
- [24] Norris, D.J., 1968. Correlation of solar radiation with clouds. *Sol. Energy* 12 (1), 107–112.
- [25] Wen, G., Cahalan, R.F., Tsay, S.-C., Oreopoulos, L., 2001. Impact of cumulus cloud spacing on Landsat atmospheric correction and aerosol retrieval. *J. Geophys. Res. Atmos.* 106 (D11), 12129–12138.
- [26] G.M. Neves, W.A. Vilela, E.B. Pereira, et al. Influência do espectro solar em módulos fotovoltaicos sob céu limpo, céu parcialmente nublado e céu nublado. *Congresso Brasileiro de Energia Solar - CBENS*, <https://anaiscbens.emnuvens.com.br/cbens/article/view/257> (2018, accessed 13 September 2022).
- [27] B.R. Paudyal, A.G. Imenes, Analysis of spectral irradiance distribution for PV applications at high latitude. In: *2020 47th IEEE Photovoltaic Specialists Conference (PVSC)*. 2020, pp. 1834–1841.
- [28] M. Zamora Zapata, E. Wu, J. Kleissl, Irradiance Enhancement Events in the Coastal Stratocumulus Dissipation Process. In: *Proceedings of the ISES Solar World Congress 2019*. Santiago, Chile: International Solar Energy Society, pp. 1–8.
- [29] Pecenak, Z.K., Mejia, F.A., Kurtz, B., Evan, A., Kleissl, J., 2016. Simulating irradiance enhancement dependence on cloud optical depth and solar zenith angle. *Sol. Energy* 136, 675–681.
- [30] Yordanov, G.H., 2015. A study of extreme overirradiance events for solar energy applications using NASA's I3RC Monte Carlo radiative transfer model. *Sol. Energy* 122, 954–965.
- [31] Calbó, J., González, J.-A., Badosa, J., et al., 2017. How large and how long are UV and total radiation enhancements? *AIP Conf. Proc.* 1810, 110002.
- [32] A.A. Kokhanovsky, A. Smirnov, S.V. Korkin, et al. The retrieval of cloud properties based on spectral solar light diffuse transmittance measurements under optically

- thick cloud cover conditions. *J. Quantitative Spectroscopy Radiative Transfer* 2020; 251: 107008.
- [33] Feister, U., Cabrol, N., Häder, D., 2015. UV irradiance enhancements by scattering of solar radiation from clouds. *Atmos.* 6, 1211–1228.
- [34] Mateos, D., 2012. Cloud modulation of shortwave and ultraviolet solar irradiances at surface. *Opt Pura Apl* 45, 29–32.
- [35] Neves, G., Vilela, W., Pereira, E., Yamasoe, M., Nofuentes, G., 2021. Spectral impact on PV in low-latitude sites: the case of southeastern Brazil. *Renew. Energy* 164, 1306–1319.
- [36] Martín, N., Ruiz, J.M., 1999. A new method for the spectral characterisation of PV modules. *Prog Photovolt. Res. Appl.* 7 (4), 299–310.
- [37] W. Holmgren, R. Andrews, A. Lorenzo, et al., *PVLIB Python 2015*. 2015.
- [38] W.F. Holmgren, D.G. Groenendyk, An open source solar power forecasting tool using PVLIB-Python. In: *2016 IEEE 43rd Photovoltaic Specialists Conference (PVSC)*. Portland, OR, USA: IEEE, pp. 0972–0975.
- [39] J. Stein, W. Holmgren, J. Forbess, et al. *PVLIB: Open source photovoltaic performance modeling functions for Matlab and Python*. 2016.
- [40] Holmgren, W.F., Hansen, C.W., Mikofski, M.A., 2018. pvlib python: a python package for modeling solar energy systems. *JOSS* 3 (29), 884.
- [41] Yoshida, S., Ueno, S., Kataoka, N., Takakura, H., Minemoto, T., 2013. Estimation of global tilted irradiance and output energy using meteorological data and performance of photovoltaic modules. *Sol. Energy* 93, 90–99.
- [42] Lohmann, G.M., 2018. Irradiance variability quantification and small-scale averaging in space and time: a short review. *Atmos.* 9, 264.
- [43] A. Louwen, A.C. de Waal, van Sark WGJHM. Evaluation of different indicators for representing solar spectral variation. In: *2016 IEEE 43rd Photovoltaic Specialists Conference (PVSC)*. 2016, pp. 0133–0137.
- [44] Nofuentes, G., Guemard, C.A., Aguilera, J., Pérez-Godoy, M.D., Chartre, F., 2017. Is the average photon energy a unique characteristic of the spectral distribution of global irradiance? *Sol. Energy* 149, 32–43.
- [45] Nofuentes, G., Guemard, C.A., Caballero, J.A., Marques-Neves, G., Aguilera, J., 2021. Experimental evaluation of a spectral index to characterize temporal variations in the direct normal irradiance spectrum. *Appl. Sci.* 11 (3), 897.
- [46] C.N. Jardine, R. Gottschalg, T. Betts, et al. *Influence of Spectral Effects on the Performance of Multijunction Amorphous Silicon Cells*. 2002.
- [47] Minemoto, T., Nakada, Y., Takahashi, H., Takakura, H., 2009. Uniqueness verification of solar spectrum index of average photon energy for evaluating outdoor performance of photovoltaic modules. *Sol. Energy* 83 (8), 1294–1299.
- [48] Norton, M., Amillo, A.M.G., Galleano, R., 2015. Comparison of solar spectral irradiance measurements using the average photon energy parameter. *Sol. Energy* 120, 337–344.
- [49] D.L. King, J.A. Kratochvil, W.E. Boyson, Measuring solar spectral and angle-of-incidence effects on photovoltaic modules and solar irradiance sensors. In: *Conference Record of the Twenty Sixth IEEE Photovoltaic Specialists Conference - 1997*. Anaheim, CA, USA: IEEE, pp. 1113–1116.
- [50] Marion, B., 2017. Numerical method for angle-of-incidence correction factors for diffuse radiation incident photovoltaic modules. *Sol. Energy* 147, 344–348.
- [51] Guemard, C.A., Lara-Fanego, V., Sengupta, M., Xie, Y.u., 2019. Surface albedo and reflectance: Review of definitions, angular and spectral effects, and intercomparison of major data sources in support of advanced solar irradiance modeling over the Americas. *Sol. Energy* 182, 194–212.
- [52] Kirn, B., Topic, M., 2017. Diffuse and direct light solar spectra modeling in PV module performance rating. *Sol. Energy* 150, 310–316.
- [53] Minemoto, T., Toda, M., Nagae, S., Gotoh, M., Nakajima, A., Yamamoto, K., Takakura, H., Hamakawa, Y., 2007. Effect of spectral irradiance distribution on the outdoor performance of amorphous Si//thin-film crystalline Si stacked photovoltaic modules. *Sol. Energy Mater. Sol. Cells* 91 (2-3), 120–122.